Available online at www.sciencedirect.com
ScienceDirect
International Journal of Thermal Sciences 46 (2007) 1084–1094
International Journal of Thermal Sciences
www.elsevier.com/locate/ijts

A numerical study of single-phase convective heat transfer in microtubes for slip flow

Wei Sun [a], Sadik Kakac [a,*], Almila G. Yazicioglu [b]

[a] *University of Miami, Coral Gables, FL 33124, USA*
[b] *Middle East Technical University, Ankara 06531, Turkey*

Received 27 September 2006; received in revised form 12 January 2007; accepted 12 January 2007

Available online 2 March 2007

Abstract

The steady-state convective heat transfer for laminar, two-dimensional, incompressible rarefied gas flow in the thermal entrance region of a tube under constant wall temperature, constant wall heat flux, and linear variation of wall temperature boundary conditions are investigated by the finite-volume finite difference scheme with slip flow and temperature jump conditions. Viscous heating is also included, and the solutions are compared with theoretical results where viscous heating has been neglected. For these three boundary conditions for a given Brinkman number, viscous effects are presented in the thermal entrance region along the channel. The effects of Knudsen and Brinkman numbers on Nusselt number are presented in graphical and tabular forms in the thermal entrance region and under fully developed conditions.

Keywords: Microscale heat transfer; Microtubes; Slip flow

1. Introduction

Devices having dimensions of the order of micrometers are being developed for use in the cooling of integrated circuits (ICs), biochemical applications, microelectromechanical systems (MEMS), and cryogenics. The use of higher densities and frequencies in microelectronic circuits for computers is increasing day by day. The trend of miniaturization has significantly aggravated the problem associated with the overheating of ICs. They require effective cooling from a relatively low surface area. This requires efficient thermal design; increasing scales of circuit integration of electronic components accompanied by reducing feature size of IC chips tremendously increased the problem associated with the dissipation of the generated heat. With existing heat flux levels exceeding 100 W/cm^2, new thermal control methods have become mandatory. These trends in thermal packaging have been discussed in [1,2]. Hence, the development of efficient cooling techniques associated with microelectric devices is one of the important contemporary applications of microscale heat transfer. This pressing requirement has initiated extensive research in microchannel cooling; experimental as well as analytic methods are reported for predicting the flow and temperature of the coolant, which is essential for chip thermal design and for microdevices.

There are basically two ways of modeling a flow field; either as the fluid really is—a collection of molecules—or as a continuum where the matter is assumed continuous and indefinitely divisible. The former modeling is subdivided into deterministic methods and probabilistic ones, while in the latter approach velocity, density, pressure, etc., are defined at every point in space and time, and conservation of mass, energy, and momentum lead to a set of nonlinear partial differential equations (Navier–Stokes).

Over the last few years considerable attention has been given to heat transfer in microchannels due to the extraordinary advantages for practical applications in microdevices. A detailed survey of the literature is given by Yener et al. [3]. Comprehensive reviews on the convective heat transfer through microchannels are also given by Morini [4].

Navier–Stokes-based fluid dynamics solvers are often inaccurate when applied to MEMS. This inaccuracy stems from

* Corresponding author.
E-mail address: skakac@miami.edu (S. Kakac).

1290-0729/$ – see front matter
doi:10.1016/j.ijthermalsci.2007.01.020

Nomenclature

A	temperature coefficient	K/m
$\bar{A}$	temperature coefficient, $AL/(T_0 - T_{s0})$	
Br	Brinkman number, $Ec\,Pr$, $\mu u_m^2/k\Delta T$	
Br^*	Brinkman number, $\mu u_m^2/q_w D$	
c_p	specific heat at constant pressure	J/kg K
c_v	specific heat at constant volume	J/kg K
D	diameter of the tube	m
D_h	hydraulic diameter	m
Ec	Eckert number, $u_m^2/c_p\Delta T$	
F_m	momentum accommodation coefficient	
F_t	thermal accommodation coefficient	
Gz	Graetz number, $Re\,Pr\,D_h/L$	
h	heat transfer coefficient	W/m^2 K
k	thermal conductivity	W/m K
Kn	Knudsen number, λ/D_h	
L	channel length	m
Nu	Nusselt number, hD_h/k	
P	pressure	Pa
Pr	Prandtl number, ν/α	
q_w	wall heat flux	W/m^2
R	radius of the tube	m
$\Re$	gas constant	
r	radial coordinate	m
Re	Reynolds number, $\rho D_h u_m/\mu$	
T	temperature	K
ΔT	temperature difference, $T_0 - T_{s,0}$	K
u	axial velocity	m/s
u^*	dimensionless axial velocity	
V	volume	m^3
ΔV	differential volume	m^3
x	axial coordinate	m

Greek symbols

α	thermal diffusivity	m^2/s
γ	heat capacity ratio, c_p/c_v	
ζ	dimensionless x	
η	dimensionless radius	
θ	dimensionless temperature, cwt	
$\bar{\theta}$	dimensionless temperature, Lwt	
θ^*	uniform wall temperature, chf	
λ	molecular mean free path	m
μ	dynamic viscosity	kg/ms
ν	kinematic viscosity	m^2/s
ρ	density	kg/m^3

Subscripts

b	bulk
chf	constant heat flux
cwt	constant wall temperature
Lwt	linear wall temperature
m	mean
o	inlet
s	fluid properties at the surface
w	wall
x	local values

their calculation of molecular transport effects, such as viscous dissipation and thermal conduction, from bulk flow quantities, such as mean velocity and temperature. This approximation of microscale phenomena with macroscale information fails as the characteristic length of the gaseous flow gradients (L) approaches the average distance traveled by molecules between collisions (the mean free path, λ). The ratio of these quantities is known as Knudsen number, Kn, which defines flow characteristics when the flow dimensions approach the molecular mean free path.

$$Kn = \frac{\lambda}{L} \tag{1}$$

In a microtube, the characteristic length is the hydraulic diameter, D_h, thus, $Kn = \lambda/D_h$. Generally the traditional continuum approach is valid, albeit with modified boundary conditions as long as $Kn < 0.1$. For small values of Kn ($Kn \leqslant 10^{-3}$), the fluid exhibits continuum behavior and can be analyzed by the Navier–Stokes equation with no-slip flow boundary conditions, while for larger values of Kn ($Kn \geqslant 10$), the fluid is considered to be in free molecular flow. For $10^{-3} < Kn < 10^{-1}$, the fluid is in the slip flow regime, and when $0.1 < Kn < 10$, the flow is assumed to be in the transitional region [3].

Tuckerman and Pease [5] first demonstrated that a water-cooled microchannel heat sink is capable of dissipating a heat flux of 790 W/cm^2 without any phase change. The authors noted that convective heat transfer coefficient, h, for laminar flow through microchannels might be higher than for turbulent flow through conventionally sized microchannels. Since then there has been an unprecedented upsurge of research in convection through microchannels. Major research initiatives are being launched to improve our fundamental understanding of the phenomena at the microscale wherein certain effects, which are generally ignored at the macroscale, become predominant.

Beskok et al. [6] presented models and a computational methodology of simulating gas microflow in the slip flow region for Knudsen number less than 0.3. Yu and Ameel [7] studied laminar slip-flow forced convection in rectangular microchannels analytically by applying a modified generalized integral transform technique to solve the energy equation, assuming hydrodynamically fully developed flow.

Convective heat transfer analysis for a gaseous flow in microchannels was performed by Hadjiconstantinou [8] for a Knudsen number range of 0.06–1.1. In this range, the flow is mostly called transition flow. Since the continuum assumption is not valid, the Direct Simulation Monte Carlo (DSMC) technique was applied. Larrode et al. [9] solved heat convection for gaseous flows in circular tubes in the slip flow regime

with uniform temperature boundary condition. The effects of rarefaction and surface accommodation coefficient were considered. Tunc and Bayazitoglu [10,11] studied convective heat transfer for steady state, laminar, hydrodynamically developed flow in microtubes with uniform temperature and uniform heat flux boundary conditions by the use of the integral transform technique. In another paper, Tunc and Bayazitoglu [12] analyzed heat transfer by convection in a rectangular microchannel. The flow was assumed to be fully developed both thermally and hydrodynamically. The H2-type boundary condition, constant axial and peripheral heat flux, was applied at the walls of the channel. Bayazitoglu and Kakac [13] discussed the flow regimes and the dimensionless parameters that affect the flow field in microchannel single phase gaseous fluid flow. The authors noted that viscous heating, compressibility, and rarefaction are to be considered in gaseous flows in microchannels. Hadjiconstantinou and Simek [14] investigated the constant-wall-temperature heat transfer characteristics of a model gaseous flow in two-dimensional micro- and nanochannels under hydrodynamically and thermally fully developed conditions. Both the slip-flow regime and the transition regime were covered. A detailed numerical simulation of forced convection heat transfer occurring in silicon-based microchannel heat sinks was conducted by Li et al. [15] using a simplified three-dimensional conjugate heat transfer model (2D fluid flow and 3D heat transfer). Mikhailov et al. [16] solved the steady state heat transfer in thermally developing, hydrodynamically developed forced laminar flow inside microconduits with uniform and periodic inlet temperature, and the steady-state heat transfer in thermally and hydrodynamically developed electroosmotic flow inside microconduits with uniform wall heat flux and inlet temperature by using Mathematica software. Tso and Mahulikar [17] proposed the use of Brinkman number to explain the unusual behavior of laminar liquid flow in microchannels and experimentally verified that Brinkman number correlates the convection in microchannels in spite of its relatively low values, and also decides the fundamental limit for the reduction of the microchannel dimensions (for optimum design).

Aydin and Avci [18] studied and presented an analytical solution to laminar forced convection in a microchannel between two parallel plates under fully developed conditions. Solutions to the energy equation are given for slip flow under constant wall temperature and constant wall heat flux boundary conditions, considering the effect of the viscous dissipation.

The objectives of this study are to numerically investigate two-dimensional single-phase forced convection for gaseous slip flow in a microtube under constant wall heat flux, constant wall temperature, and linearly varying wall temperature boundary conditions, and to investigate the effects of Brinkman number and Knudsen number on Nusselt number. An algorithm will be developed for future use under these three boundary conditions including the effect of viscous dissipation. The numerical method will be verified by comparing it with analytical results available for simplified cases in the literature.

2. Slip velocity and temperature jump

As a result of slip velocity and temperature jump conditions, the fluid particles adjacent to the solid surface no longer attain the velocity and the temperature of the solid surface. Therefore, the fluid particles have a tangential velocity at the surface, which is the slip velocity, and it is expressed as [6]

$$u_s = -\frac{2-F_m}{F_m}\lambda\left(\frac{\mathrm{d}u}{\mathrm{d}r}\right)_{r=R} + 3\sqrt{\frac{\Re T}{8\pi}}\frac{\lambda}{T}\left(\frac{\partial T}{\partial x}\right)_{r=R} \tag{2}$$

In Eq. (2), thermal creep, which accounts for fluid flow induced by the temperature gradient, is neglected; this term is second order in Knudsen number [6]. Therefore, for the moderate temperature gradients, the second term is negligible for low Knudsen numbers, which is the case for slip flow regime. If the surface is absolutely smooth and reflects the molecules specularly, the tangential momentum will not change, and F_m will be equal to zero. Molecules can also be reflected diffusely, which results in $F_m = 1$. This means that all the tangential momentum is lost at the wall [9]. Diffuse reflection results from the penetration of the molecules into the interstices in the surface, where multiple strikes occur before the molecule leaves, and from surface roughness. Accommodation coefficient may be significantly different from unity for light atoms and closer to unity for heavy atoms.

The fluid particles have a finite temperature difference at the solid surface (temperature jump). Neglecting thermal creep, as was done in Eq. (2), temperature jump can be expressed as

$$T_s - T_w = -\frac{2-F_t}{F_t}\frac{2\gamma}{(\gamma+1)Pr}\lambda\left(\frac{\mathrm{d}T}{\mathrm{d}r}\right)_{r=R} \tag{3}$$

where the thermal accommodation coefficient, F_t, is defined as

$$F_t = \frac{E_a - E_l}{E_a - E_w} \tag{4}$$

where E_a is the energy of the approaching stream, E_l is the energy carried by the molecules leaving the surface, and E_w is the energy of the molecules leaving the surface at the wall temperature.

3. Analysis

With coordinates shown in Fig. 1, the fully developed velocity profile can be determined by solving the equation of motion for a steady and fully-developed laminar flow of a viscous fluid

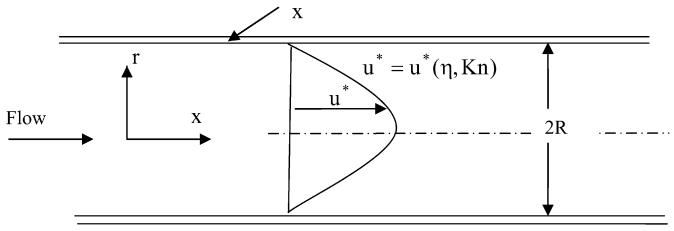

Fig. 1. Geometry of the problem.

in a tube [3] with the use of the slip velocity, Eq. (2), at the wall and the symmetry condition at the centerline of the tube as

$$\frac{u}{u_m} = \frac{2[1-(r/R)^2]+8Kn}{1+8Kn} \tag{5}$$

3.1. Constant wall temperature

The steady-state energy equation for laminar flow under the fully developed velocity condition (Poiseuille flow) with constant fluid properties, including heat dissipation, can be written as [19]

$$u\frac{\partial T}{\partial x} = \frac{\alpha}{r}\frac{\partial}{\partial r}\left(r\frac{\partial T}{\partial r}\right) + \frac{\nu}{c_p}\left(\frac{\mathrm{d}u}{\mathrm{d}r}\right)^2 \tag{6}$$

$$\text{At } r = R, \quad T = T_s \tag{6a}$$

$$\text{at } r = 0, \quad \frac{\partial T}{\partial r} = 0 \tag{6b}$$

$$\text{at } x = 0, \quad T = T_0 \tag{6c}$$

where T_0 and T_s are the temperature of the gas at the inlet and at the surface, respectively.

The energy equation (6) can be made dimensionless by defining the following dimensionless parameters:

$$\theta = \frac{T-T_s}{T_0-T_s}, \qquad \eta = \frac{r}{R}, \qquad \zeta = \frac{x}{L}$$

$$u^* = \frac{u}{u_m} = \frac{2(1-\eta^2+4Kn)}{1+8Kn} \tag{6d}$$

Then, we obtain the following dimensionless form of Eq. (6) and the boundary conditions:

$$\frac{Gz(1-\eta^2+4Kn)}{2(1+8Kn)}\frac{\partial\theta}{\partial\zeta} = \frac{1}{\eta}\frac{\partial}{\partial\eta}\left(\eta\frac{\partial\theta}{\partial\eta}\right) + \frac{16Br}{(1+8Kn)^2}\eta^2 \tag{7}$$

$$\text{At } \eta = 1, \quad \theta = 0 \tag{7a}$$

$$\text{at } \eta = 0, \quad \frac{\partial\theta}{\partial\eta} = 0 \tag{7b}$$

$$\text{at } \zeta = 0, \quad \theta = 1 \tag{7c}$$

Brinkman number, $Br = \mu u_m^2/(T_0 - T_{s0})$, is the ratio of heat generated by viscous dissipation to heat transferred by conduction over the cross-section. Brinkman number also emerges from the dimensionless general energy equation as the product of Eckert ($u_m^2/c_p\Delta T$) and Prandtl (ν/α) numbers. Negative values of Br means that the fluid is being cooled.

Heat transfer from the wall to the fluid by convection is written as

$$q_w = h_x(T_w - T_b) \tag{8}$$

where the bulk temperature of the fluid along the tube for an incompressible fluid with constant specific heat is defined as

$$T_b = \frac{\int_A T u\,\mathrm{d}A}{\int_A u\,\mathrm{d}A} \tag{9}$$

Heat flux at the wall can also be written using Fourier's law of heat conduction:

$$q_w = k\left.\frac{\partial T}{\partial r}\right|_{r=R} \tag{10}$$

Nusselt number can be obtained for the constant wall temperature as [13]:

$$Nu_x = \frac{h_x D}{k} = -\frac{2\frac{\partial\theta}{\partial\eta}\big|_{\eta=1}}{\left(\theta_b - \frac{4\gamma}{\gamma+1}\frac{Kn}{Pr}\frac{\partial\theta}{\partial\eta}\big|_{\eta=1}\right)} \tag{11}$$

where θ_b is the dimensionless bulk temperature, which can be obtained from Eq. (9) as:

$$\theta_b = 2\int_0^1 \left(\frac{u}{u_m}\right)\theta(\eta,\zeta)\eta\,\mathrm{d}\eta \tag{12}$$

3.2. Constant heat flux

For this condition, the energy equation and the boundary conditions become

$$u\frac{\partial T}{\partial x} = \frac{\alpha}{r}\frac{\partial}{\partial r}\left(r\frac{\partial T}{\partial r}\right) + \frac{\nu}{c_p}\left(\frac{\mathrm{d}u}{\mathrm{d}r}\right)^2 \tag{13}$$

$$\text{At } r = R, \quad k\frac{\partial T}{\partial r} = q_w \tag{13a}$$

$$\text{at } r = 0, \quad \frac{\partial T}{\partial r} = 0 \tag{13b}$$

$$\text{at } x = 0, \quad T = T_0 \tag{13c}$$

The energy equation (13) can be made dimensionless by defining $\theta = \frac{T-T_0}{q_w R/k}$:

$$\frac{Gz(1-\eta^2+4Kn)}{2(1+8Kn)}\frac{\partial\theta^*}{\partial\zeta} = \frac{1}{\eta}\frac{\partial}{\partial\eta}\left(\eta\frac{\partial\theta^*}{\partial\eta}\right) + \frac{32Br^*}{(1+8Kn)^2}\eta^2 \tag{14}$$

$$\text{At } \eta = 1, \quad \frac{\partial\theta^*}{\partial\eta} = 1 \tag{14a}$$

$$\text{at } \eta = 0, \quad \frac{\partial\theta^*}{\partial\eta} = 0 \tag{14b}$$

$$\text{at } \zeta = 0, \quad \theta^* = 0 \tag{14c}$$

where Br^* is defined as $Br^* = \frac{\mu u_m^2}{q_w D}$.

Similarly, we can derive an expression for the local Nusselt number as above [13]:

$$Nu_x = \frac{h_x D}{k} = \frac{2}{\theta_s^* + \frac{4\gamma}{\gamma+1}\frac{Kn}{Pr} - \theta_b^*} \tag{15}$$

3.3. Linear wall temperature

For this condition, the energy equation and the boundary conditions become

$$u\frac{\partial T}{\partial x} = \frac{\alpha}{r}\frac{\partial}{\partial r}\left(r\frac{\partial T}{\partial r}\right) + \frac{\nu}{c_p}\left(\frac{\mathrm{d}u}{\mathrm{d}r}\right)^2 \tag{16}$$

$$\text{At } r = R, \quad T = T_s(x) = T_{s0} + Ax \tag{16a}$$

$$\text{at } r = 0, \quad \frac{\partial T}{\partial r} = 0 \tag{16b}$$

$$\text{at } x = 0, \quad T = T_0 \tag{16c}$$

where $T_{s0} = T_s|_{x=0}$ and $T_s(x) - T_w(x) = -\frac{2-F_t}{F_t}\frac{2\gamma}{(\gamma+1)Pr} \times \lambda(\frac{\mathrm{d}T}{\mathrm{d}r})_{r=R}$.

Introducing $\bar{\theta} = \frac{T-T_{s0}}{T_0-T_{s0}}$, the dimensionless form of the energy equation can be written as follows:

$$\frac{Gz(1-\eta^2+4Kn)}{2(1+8Kn)}\frac{\partial\bar{\theta}}{\partial\zeta} = \frac{1}{\eta}\frac{\partial}{\partial\eta}\left(\eta\frac{\partial\bar{\theta}}{\partial\eta}\right) + \frac{16Br}{(1+8Kn)^2}\eta^2 \quad (17)$$

$$\text{At } \eta = 1, \quad \bar{\theta} = \bar{A}\varsigma \quad (17a)$$

$$\text{at } \eta = 0, \quad \frac{\partial\bar{\theta}}{\partial\eta} = 0 \quad (17b)$$

$$\text{at } \zeta = 0, \quad \bar{\theta} = 1 \quad (17c)$$

where $\bar{A} = \frac{AL}{T_0-T_{s0}}$, $Br = \frac{\mu u_m^2}{k\Delta T}$, and $\Delta T = T_0 - T_{s0}$ is the temperature difference between the fluid at tube entrance and at the wall when $x = 0$.

Similarly, the local Nusselt number considering the temperature jump can be obtained as:

$$Nu_x = \frac{h_x D}{k} = -\frac{2\frac{\partial\bar{\theta}}{\partial\eta}\big|_{\eta=1}}{\left(\bar{\theta}_b - \frac{4\gamma}{\gamma+1}\frac{Kn}{Pr}\frac{\partial\bar{\theta}}{\partial\eta}\big|_{\eta=1} - \bar{A}\varsigma\right)} \quad (18)$$

4. Numerical method

The finite control volume-finite difference method is used to solve the energy equation based on Patankar method [20]. In the solutions of the coupled algebraic equations, the Alternate Direction Iteration (ADI) and Tridiagonal Matrix Algorithm (TDMA) are applied along the tube and in radial directions; in the axial direction, forward difference, and in the radial direction central difference is used. In both directions, 1000 nodes are computed. The implicit method is applied to compute the temperature profile, since this method is always stable and the convergence is guaranteed. The grid sizes are clustered in the thermal entrance region and near the wall for better accuracy of the solutions and the temperature gradient near the wall. It is found that the solutions are grid independent. A code is written in Fortran-90 for future use. Referring to Fig. 2, one can write the following for a control volume P:

$$\Delta V_p = \frac{\eta_n+\eta_s}{2}\Delta\eta_P, \qquad \eta_P = \frac{1}{2}(\eta_n+\eta_s)$$
$$\eta_S = \eta_P - \frac{1}{2}\Delta\eta_P, \qquad \eta_N = \eta_P + \frac{1}{2}\Delta\eta_P \quad (19)$$

Multiplying energy equation (7) by η and integrating it over the selected control volume, we obtain:

$$\frac{Gz}{2(1+8Kn)\Delta\zeta}\left(1+4Kn-\frac{\eta_n^2+\eta_s^2}{2}\right)(\theta_P-\theta_P^0) = \frac{1}{\Delta V}\left(\eta_n\frac{\theta_N-\theta_P}{\eta_N-\eta_P} - \eta_s\frac{\theta_P-\theta_S}{\eta_P-\eta_S}\right) + \frac{16Br}{(1+8Kn)^2}\frac{\eta_n^2+\eta_s^2}{2} \quad (20)$$

To simplify Eq. (20), we can write the following:

$$a_N = \frac{\eta_n}{\eta_N-\eta_P}, \qquad a_S = \frac{\eta_s}{\eta_P-\eta_S}$$
$$a_P^0 = \frac{\frac{Gz}{2(1+8Kn)}(1+4Kn-\frac{\eta_n^2+\eta_s^2}{2})}{\Delta\zeta}\Delta V \quad (21)$$

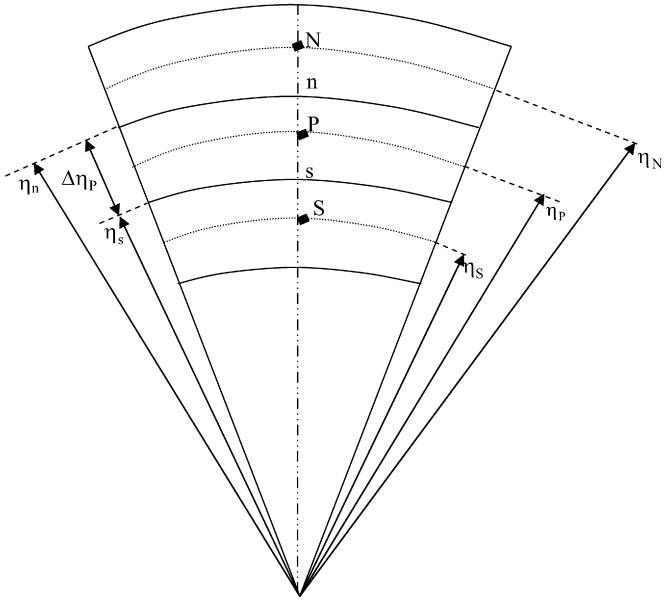

Fig. 2. Control volume.

$$a_P = a_N + a_S + a_P^0 \quad (22)$$

Then Eq. (20) can be written as:

$$a_P\theta_P = a_N\theta_N + a_S\theta_S + b \quad (23)$$

where

$$b = S_c\Delta V \quad \text{and} \quad S_c = \frac{16Br}{(1+8Kn)^2}\frac{\eta_n^2+\eta_s^2}{2} + \frac{a_P^0\theta_P^0}{\Delta V} \quad (24)$$

for constant wall temperature and linear wall temperature boundary conditions.

Multiplying energy equation (14) by η and integrating it over the selected control volume, we can also obtain the same form of equations as Eq. (23), except for S_c, which is

$$S_c = \frac{32Br}{(1+8Kn)^2}\frac{\eta_n^2+\eta_s^2}{2} + \frac{a_P^0\theta_P^0}{\Delta V} \quad (25)$$

for constant heat flux boundary conditions.

For the boundary control volume, the temperature of the node on the line is known.

When $\eta = 0$,

$$a_S' = 0, \qquad a_P' = a_S' + a_N + a_P^0, \qquad b' = b \quad (26)$$

when $\eta = 1$,

$$a_N' = 0, \qquad a_P' = a_S + a_N' + a_P^0 \quad (27)$$

$$b' = b + a_N\theta|_{\eta=1} = b$$

for constant wall temperature (28)

$$b' = b + a_N\theta|_{\eta=1} = b + a_N\bar{A}\zeta_P$$

for linear wall temperature (29)

$$b' = b + \eta\frac{\partial\theta}{\partial\eta}\bigg|_{\eta=1} = b + 1$$

for constant heat flux. (30)

With the problem formulated as above, the temperature distribution for each point along the axial line, the temperature

gradient on the wall and the Nusselt numbers can then be calculated [20,21].

5. Results and discussion

In this section, the effects of Knudsen number, temperature jump, and positive/negative Brinkman number on heat transfer under different boundary conditions are presented. The analytical (Ref. [10]) and numerical results for constant wall temperature and constant heat flux boundary conditions with no viscous heating are compared in Tables 1 and 2, which is the validation of the accuracy of the numerical code developed.

Table 1
Developed conditions, laminar flow Nusselt number values (T_w = constant, $Pr = 0.6$)

$Br = 0$	Nu_T (analytical) [10]	Nu_T (numerical)
$Kn = 0.0$	3.6751	3.6566
$Kn = 0.02$	3.3675	3.3527
$Kn = 0.04$	3.0745	3.0627
$Kn = 0.06$	2.8101	2.8006
$Kn = 0.08$	2.5767	2.5689
$Kn = 0.10$	2.3723	2.3659
$Kn = 0.12$	2.1937	2.1882

Table 2
Developed conditions, laminar flow Nusselt number values (q_w = constant, $Pr = 0.6$)

$Br = 0$	Nu_q (analytical) [10]	Nu_q (numerical)
$Kn = 0.0$	4.3627	4.3649
$Kn = 0.02$	3.9801	4.0205
$Kn = 0.04$	3.5984	3.6548
$Kn = 0.06$	3.2519	3.3126
$Kn = 0.08$	2.9487	3.0081
$Kn = 0.10$	2.6868	2.7425
$Kn = 0.12$	2.4613	2.5125

Table 3
The fully developed Nusselt number values, $Br = 0$, T_w = constant

$Br = 0.00$	$Pr = 0.6$	$Pr = 0.7$	$Pr = 0.8$	$Pr = 0.9$	$Pr = 1.0$
$Kn = 0.00$	3.6566	3.6566	3.6566	3.6566	3.6566
$Kn = 0.02$	3.3527	3.4163	3.4657	3.5050	3.5372
$Kn = 0.04$	3.0627	3.1706	3.2567	3.3269	3.3853
$Kn = 0.06$	2.8006	2.9377	3.0497	3.1429	3.2216
$Kn = 0.08$	2.5689	2.7244	2.8540	2.9636	3.0576
$Kn = 0.10$	2.3659	2.5323	2.6733	2.7944	2.8994
$Kn = 0.12$	2.1882	2.3604	2.5084	2.6371	2.7499

Table 4
The fully developed Nusselt number values, $Br = 0.01$, T_w = constant

$Br = 0.01$	$Pr = 0.6$	$Pr = 0.7$	$Pr = 0.8$	$Pr = 0.9$	$Pr = 1.0$
$Kn = 0.00$	9.5985	9.5985	9.5985	9.5985	9.5985
$Kn = 0.02$	7.1327	7.427	7.6642	7.8594	8.0229
$Kn = 0.04$	5.6525	6.0313	6.3505	6.6231	6.8587
$Kn = 0.06$	4.6708	5.0651	5.4075	5.7076	5.9727
$Kn = 0.08$	3.9744	4.3594	4.701	5.006	5.2802
$Kn = 0.10$	3.4558	3.8227	4.1535	4.4532	4.7261
$Kn = 0.12$	3.0552	3.4016	3.7177	4.0074	4.2738

The results are shown in Tables 3 and 4 for constant wall temperature boundary condition with $Br = 0$ and $Br = 0.01$, respectively. The fully developed Nusselt number decreases as Kn increases. For the no-slip condition, when $Br = 0.01$, $Nu = 9.5985$, while it drops down to 3.4016 for $Kn = 0.12$ with $Pr = 0.7$, a decrease of 64.5%. This is due to the fact that the temperature jump reduces heat transfer. As Kn increases, the temperature jump also increases; the fully developed Nusselt number is a function of the Prandtl number and increases as Pr increases. The values of Kn and Pr numbers both affect the value of the temperature jump.

For this boundary condition, Kn number increase has more influence on Nusselt number with the presence of viscous dissipation. Also, the Nusselt number has larger value for the case with viscous heating.

The results are shown in Tables 5, 6, and 7 for constant heat flux boundary condition with $Br = 0$, $Br = -0.01$, and $Br = 0.01$, respectively. The fully developed Nusselt number decreases as Kn increases. It can be observed from Table 6 that for the no-slip condition, $Nu = 4.5640$, while it drops down to 2.7468 for $Kn = 0.12$ with $Pr = 0.7$, with a decrease of 39.8%, which is similar to the case of constant wall temperature boundary condition, this is due to the fact that the temperature jump reduces heat transfer. As Kn increases, the temperature jump

Table 5
The fully developed Nusselt number values $Br = 0$, q_w = constant

$Br = 0.00$	$Pr = 0.6$	$Pr = 0.7$	$Pr = 0.8$	$Pr = 0.9$	$Pr = 1.0$
$Kn = 0.00$	4.3649	4.3649	4.3649	4.3649	4.3649
$Kn = 0.02$	4.0205	4.1088	4.1788	4.2367	4.2865
$Kn = 0.04$	3.6548	3.8036	3.9243	4.0253	4.1118
$Kn = 0.06$	3.3126	3.4992	3.6544	3.7863	3.9006
$Kn = 0.08$	3.0081	3.2163	3.3932	3.5459	3.6798
$Kn = 0.10$	2.7425	2.9616	3.151	3.3168	3.4638
$Kn = 0.12$	2.5125	2.7354	2.9309	3.1043	3.2595

Table 6
The fully developed Nusselt number values, $Br = -0.01$, q_w = constant

$Br = -0.01$	$Pr = 0.6$	$Pr = 0.7$	$Pr = 0.8$	$Pr = 0.9$	$Pr = 1.0$
$Kn = 0.00$	4.5640	4.5640	4.5640	4.5640	4.5640
$Kn = 0.02$	4.1278	4.2212	4.2953	4.3565	4.409
$Kn = 0.04$	3.7154	3.8695	3.9948	4.0995	4.1894
$Kn = 0.06$	3.3484	3.5395	3.6985	3.8338	3.9511
$Kn = 0.08$	3.0302	3.2419	3.4218	3.5772	3.7137
$Kn = 0.10$	2.7567	2.9784	3.1701	3.3381	3.4871
$Kn = 0.12$	2.5219	2.7468	2.9441	3.1191	3.2759

Table 7
The fully developed Nusselt number values, $Br = 0.01$, q_w = constant

$Br = 0.01$	$Pr = 0.6$	$Pr = 0.7$	$Pr = 0.8$	$Pr = 0.9$	$Pr = 1.0$
$Kn = 0.00$	4.1825	4.1825	4.1825	4.1825	4.1825
$Kn = 0.02$	3.9186	4.0022	4.0684	4.1233	4.1705
$Kn = 0.04$	3.5962	3.7398	3.8563	3.9536	4.0371
$Kn = 0.06$	3.2776	3.4598	3.6113	3.7399	3.8514
$Kn = 0.08$	2.9863	3.1912	3.3651	3.5151	3.6466
$Kn = 0.10$	2.7285	2.945	3.1321	3.2957	3.4408
$Kn = 0.12$	2.5031	2.7242	2.9179	3.0896	3.2432

Table 8
The fully developed Nusselt number values, $Br = 0$, $T_s = Ax + T_{s0}$ ($\bar{A} = -1$)

$Br = 0.00$	$Pr = 0.6$	$Pr = 0.7$	$Pr = 0.8$	$Pr = 0.9$	$Pr = 1.0$
$Kn = 0.00$	4.3654	4.3654	4.3654	4.3654	4.3654
$Kn = 0.02$	4.0215	4.1125	4.179	4.2377	4.2883
$Kn = 0.04$	3.6582	3.8043	3.9246	4.0339	4.1508
$Kn = 0.06$	3.327	3.5009	3.6616	3.7968	3.9179
$Kn = 0.08$	3.0229	3.2296	3.3933	3.5516	3.6852
$Kn = 0.10$	2.7427	2.9691	3.1526	3.3284	3.4938
$Kn = 0.12$	2.5264	2.7391	2.9411	3.1242	3.2825

Table 9
The fully developed Nusselt number values, $Br = 0.01$, $T_s = Ax + T_{s0}$ ($\bar{A} = -1$)

$Br = 0.01$	$Pr = 0.6$	$Pr = 0.7$	$Pr = 0.8$	$Pr = 0.9$	$Pr = 1.0$
$Kn = 0.00$	6.77	6.77	6.77	6.77	6.77
$Kn = 0.02$	5.5177	5.5479	5.5527	5.5943	5.6646
$Kn = 0.04$	4.6587	4.8019	4.9025	5.0043	5.0759
$Kn = 0.06$	4.0306	4.2312	4.3861	4.5077	4.6045
$Kn = 0.08$	3.5499	3.7791	3.9643	4.1163	4.2425
$Kn = 0.10$	3.1694	3.4111	3.6127	3.7828	3.9277
$Kn = 0.12$	2.8602	3.1055	3.3148	3.4951	3.6516

also increases; the fully developed Nusselt number increases as Pr increases. Therefore, the denominator of Eq. (15) takes smaller values.

Tables 6–7 show the effect of negative or positive Br values ($Br = \pm 0.01$), in addition to Table 5 for no viscous heating, on fully developed Nusselt numbers for constant heat flux boundary condition. From the definition of Br, for this type of boundary condition, a negative Br means that the fluid is being cooled. Therefore, the Nusselt number takes higher values for $Br < 0$ and lower values for $Br > 0$ compared with no viscous heating.

The results are shown in Tables 8 and 9 for linear wall temperature boundary condition for $Br = 0$ and $Br = 0.01$. The fully developed Nusselt number decreases as Kn increases. For the no-slip condition when $Br = 0.01$, $Nu = 6.77$, while it drops down to 3.1055 for $Kn = 0.12$ with $Pr = 0.7$, which is a decrease of 54.1%. As Kn increases, the temperature jump also increases. The fully developed Nusselt number increases as Pr increases. As Pr increases, the temperature jump decreases. Therefore, the denominator of Eq. (18) takes smaller values. It should be noted from Tables 5 and 8 that, constant heat flux and linearly varying wall temperature boundary conditions give similar values for the Nusselt number.

Under the fully developed conditions for linear wall temperature boundary condition, the fully developed Nusselt number increases as Brinkman number increases (Tables 8–9). Due to the definition of Br, the positive value means the flow is cooled. The fluid temperature becomes closer to the wall temperature as it flows through the channel. When we include viscous heating, fluid temperature takes higher values, which increases the temperature difference between the fluid and the wall, thus heat transfer.

The results, considering temperature jump, are shown in Tables 8 and 9 at $Br = 0$ and $Br = 0.01$ for cases $\bar{A} = -1$. As the temperature difference between the wall and the fluid is increased, the heat transfer is increased as well. In fact, after reaching the developed region, linear wall temperature has the same effects as constant heat flux boundary condition (Tables 8–9).

In Fig. 3, the effect of temperature jump on the Nusselt number is shown. The solid and dotted lines represent the results from the present study for constant heat flux and constant wall temperature boundary conditions, respectively. When the temperature jump condition is not considered, in other words, only the velocity slip condition is taken into account, the Nusselt number increases with increasing Kn, which implies that the velocity slip and temperature jump have opposite effects on the Nusselt number.

In Fig. 4, we show the Nusselt number values in the thermally developing region for constant wall temperature case. For both Br values, as Kn increases, the Nusselt number first decreases due to the increase in temperature jump. We note

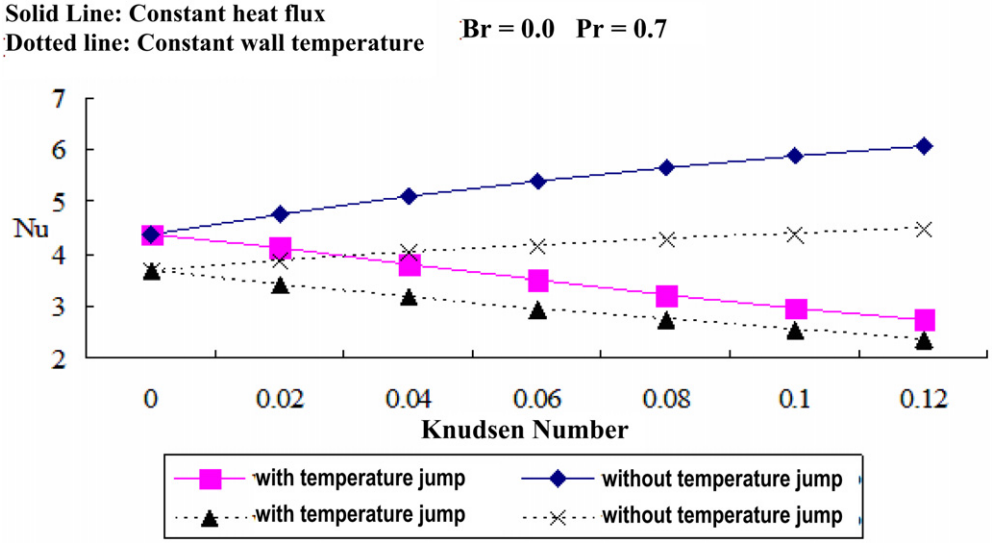

Fig. 3. The effect of temperature jump on heat transfer.

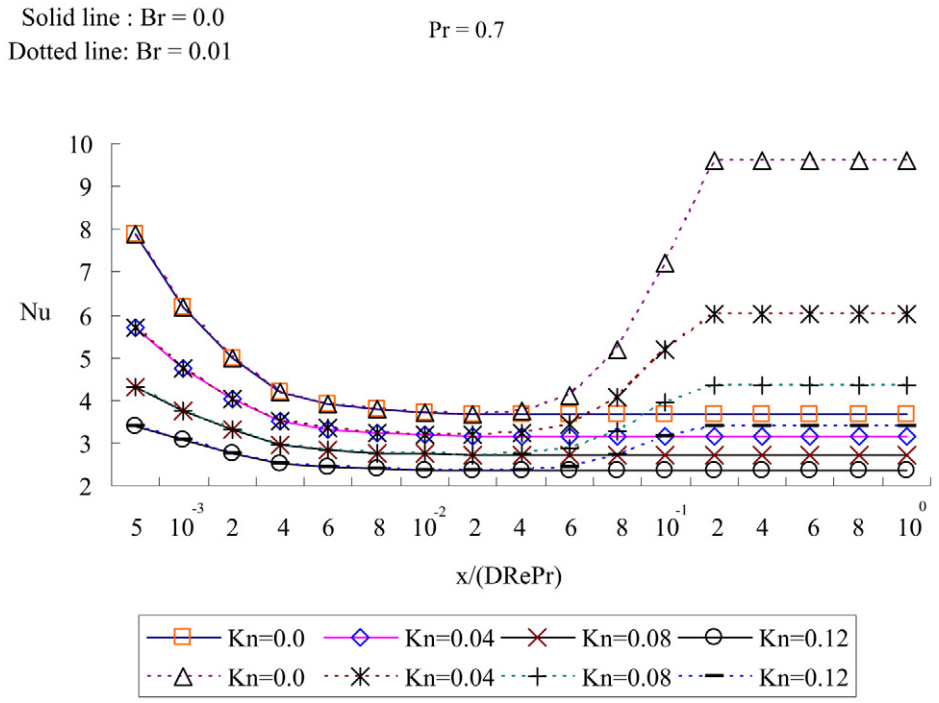

Fig. 4. Variation of Nusselt number with Knudsen number at the entrance region for constant wall temperature with temperature jump.

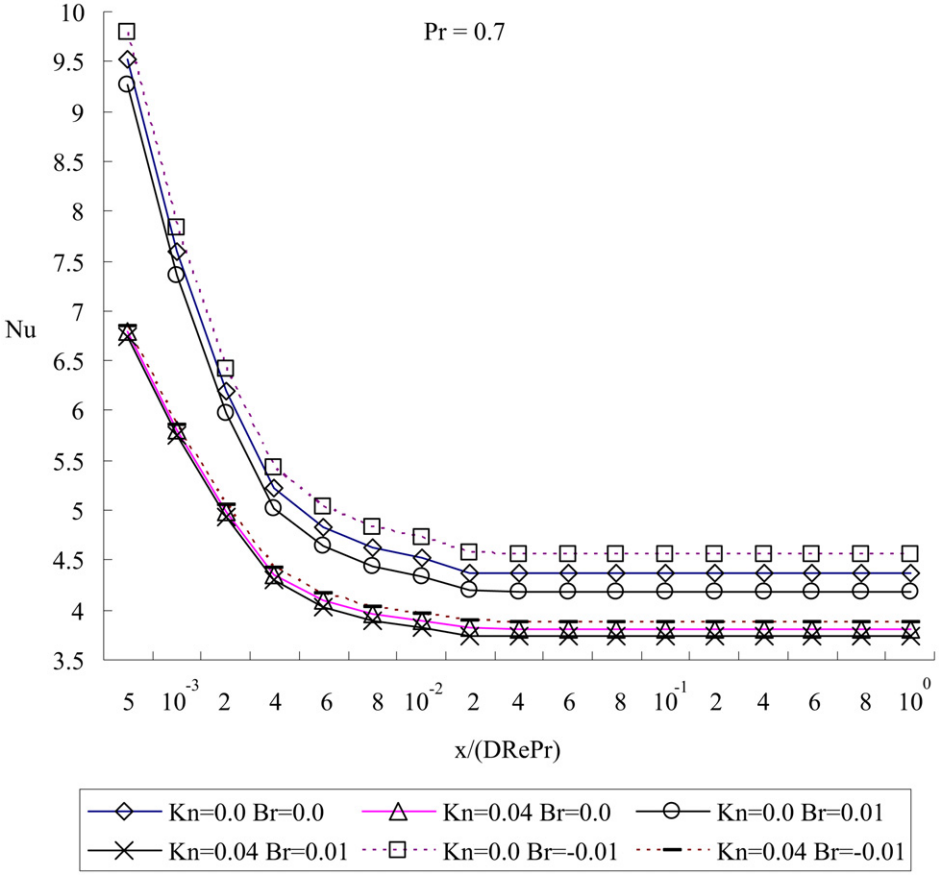

Fig. 5. Variation of Nusselt number with Knudsen number at the entrance region for constant heat flux with temperature jump.

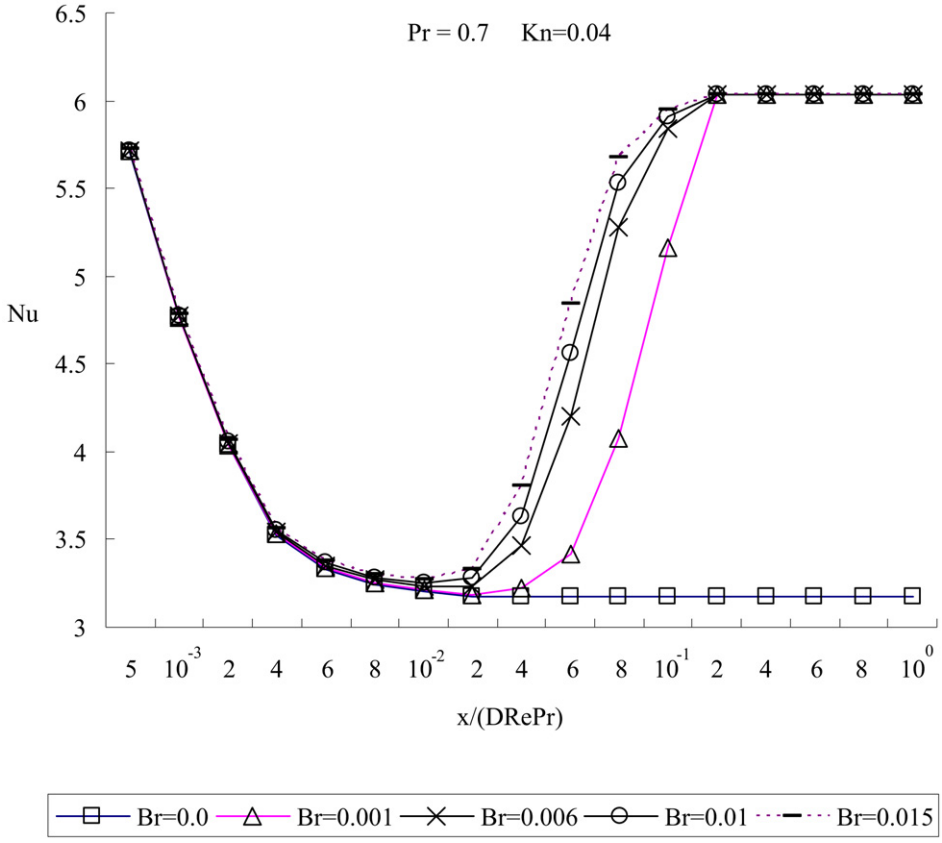

Fig. 6. Variation of Nusselt number with Brinkman number at the entrance region for constant wall temperature with temperature jump

here that, the decrease is greater for lower *Kn* values. Then, Nusselt number reaches the fully developed value as if there is no viscous heating. However, when there is viscous heating ($Br = 0.01$), at some point Nusselt number makes a jump to its final value. This final value increases with decreasing *Kn* values.

In Fig. 5, the Nusselt number values in the thermally developing region are shown for constant heat flux case. For all *Br* values, as *Kn* increases, the Nusselt number decreases due to the increase in temperature jump.

In Fig. 6, for constant wall temperature boundary condition, the system first reaches the fully developed condition as if there is no viscous heating. Then, at some point, *Nu* makes a jump to its final value. As *Br* increases, the jump occurs at a shorter distance from the entrance. Since $T_w =$ constant, the *Nu* values all converge to the same fully developed value.

Since the definition of the Brinkman number is different for the constant heat flux boundary condition case, a positive *Br* means that the heat is transferred to the fluid from the wall as opposed to the constant temperature case. Therefore, we see from Fig. 7 that *Nu* decreases as *Br* increases when $Br > 0$. Negative *Br* means the flow is cooled and *Nu* has the larger value for given *Kn* and *Pr* numbers.

6. Conclusions

In general, for the above three boundary conditions stated, velocity slip and temperature jump affect the heat transfer in opposite ways: a large slip on the wall will increase the convection along the surface. On the other hand, a large temperature jump will decrease the heat transfer by reducing the temperature gradient at the wall. Therefore, neglecting temperature jump will result in the overestimation of the heat transfer coefficient.

For constant wall temperature boundary condition considering temperature jump, the fully developed Nusselt number decreases as *Kn* increases, and is a function of the Prandtl number. Prandtl number, the increase of which increases heat transfer, is important, since it directly influences the magnitude of the temperature jump. On the other hand, without considering temperature jump and for constant wall temperature boundary condition, the fully developed Nusselt number increases as *Kn* increases, and keeps unchanged as *Pr* increases. Still, *Kn* has more influence with the presence of viscous dissipation.

In the thermal entrance region to the fully developed region, the system first reaches the fully developed condition as if there is no viscous heating. Then, at some point, *Nu* makes a jump to its final value. As *Br* increases, the jump occurs at a shorter distance from the entrance. Since the wall temperature is constant, the *Nu* values all converge to the same fully developed value, although the Nusselt number is greater for larger values of the Brinkman number in the thermal entrance region.

For constant heat flux boundary conditions with temperature jump, the fully developed Nusselt number decreases as *Kn* increases and increases as *Pr* increases. Since the definition of the Brinkman number is different for the constant heat flux boundary condition case, a positive *Br* means that the heat is

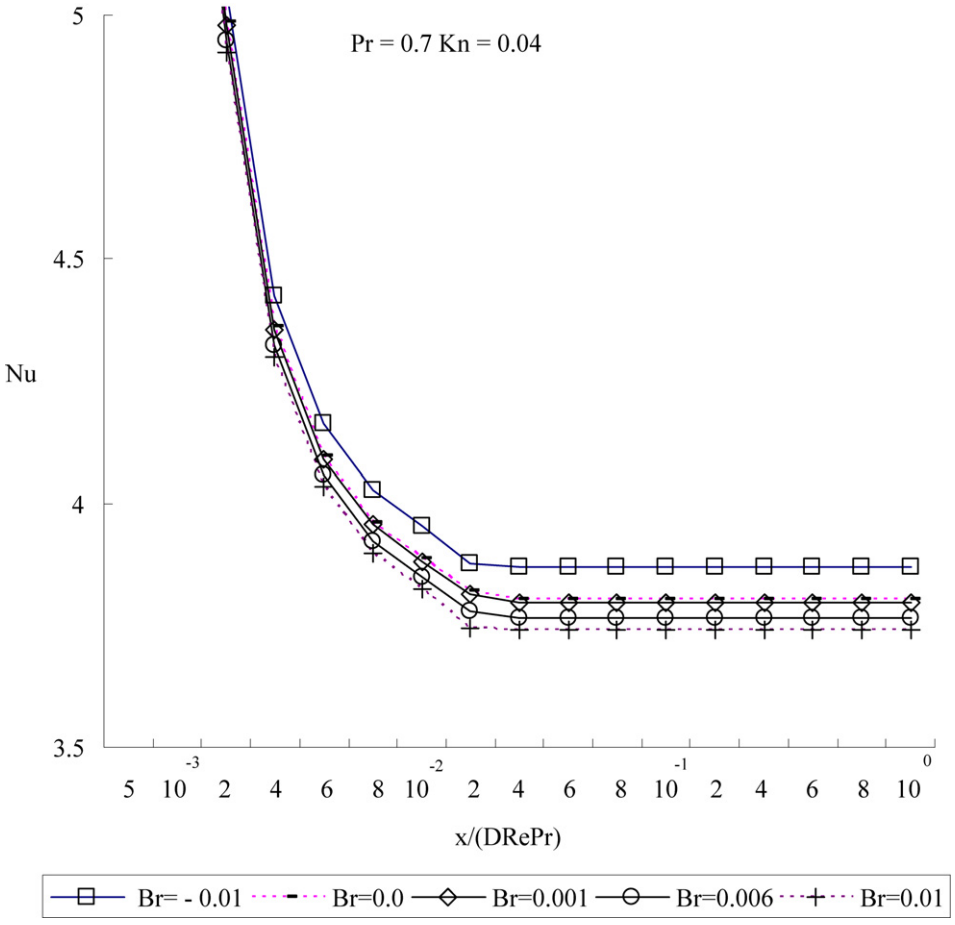

Fig. 7. Variation of Nusselt number with Brinkman number at the entrance region for constant heat flux with temperature jump.

transferred to the fluid from the wall as opposed to the constant temperature case.

The behavior of the system under linear wall temperature boundary conditions is similar to the behavior of the system under constant heat flux boundary conditions. For both these cases, the Nusselt number approaches to the value of the constant heat flux under the same conditions.

Acknowledgements

Financial support provided by the TUBITAK (Turkish Scientific and Technological Research Council) and TUBA (Turkish Academy of Sciences) is greatly appreciated. We also acknowledge the assistance provided by Mr. Basar Bulut during the preparation of this manuscript.

References

[1] A. Bar-Cohen, State of the art and trends in the thermal packaging of the electronic equipment, ASME J. Electronic Packaging 114 (1992) 257–270.
[2] S. Kakac, H. Yuncu, K. Hijkata (Eds.), Cooling of Electronic Systems, NATO ASI Series E, vol. 258, Kluwer Academic Publishers, The Netherlands, 1992.
[3] Y. Yener, S. Kakac, M. Avelino, T. Okutucu, Single phase forced convection in microchannels—state-of-the-art-review, in: S. Kakac, L. Vasiliev, Y. Bayazitoglu, Y. Yener (Eds.), Microscale Heat Transfer—Fundamentals and Applications in Biological Systems and MEMS, Kluwer Academic Publishers, The Netherlands, 2005.
[4] G.L. Morini, Single-phase convective heat transfer in microchannels: A review of experimental results, Int. J. Thermal Sci. 43 (7) (2004) 631–651.
[5] D.B. Tuckerman, R.E. Pease, Optimized convective cooling using micromachined structure, J. Electrochem. Soc. 129 (3) (1982) P.C. 98.
[6] A. Beskok, G. Em Karniadakis, W. Trimmer, Rarefaction and compressibility effects in gas microflows, J. Fluid Engrg. 118 (1996) 448–456.
[7] S.P. Yu, T.A. Ameel, Slip-flow heat transfer in rectangular microchannels, Int. J. Heat Mass Transfer 44 (22) (2001) 4225–4235.
[8] N.G. Hadjiconstantinou, Heat transfer for gaseous flow in microtubes with viscous heating, Proc. ASME Heat Transfer Division 366 (2) (2000) 1–10.
[9] F.E. Larrode, C. Housiadas, Y. Drossinos, Slip flow heat transfer in circular tubes, Int. J. Heat Mass Transfer 43 (15) (2000) 2669–2680.
[10] G. Tunc, Y. Bayazitoglu, Heat transfer for gaseous flow in microtubes with viscous heating, Proc. ASME Heat Transfer Division 366 (2) (2000) 209–306.
[11] G. Tunc, Y. Bayazitoglu, Heat transfer in microtubes with viscous dissipation, Int. J. Heat Mass Transfer 44 (13) (2001) 2395–2403.
[12] G. Tunc, Y. Bayazitoglu, Heat transfer in rectangular microchannels, Int. J. Heat Mass Transfer 45 (4) (2002) 765–773.
[13] Y. Bayazitoglu, S. Kakac, Flow regimes in microchannel single-phase gaseous fluid flow, in: S. Kakac, L. Vasiliev, Y. Bayazitoglu, Y. Yener (Eds.), Microscale Heat Transfer—Fundamentals and Applications, Kluwer Academic Publishers, The Netherlands, 2005.
[14] N.G. Hadjiconstantinou, O. Simek, Constant-wall-temperature Nusselt number in micro and nano-channels, J. Heat Transfer 124 (2) (2002) 356–364.
[15] J. Li, G.P. Peterson, P. Cheng, Three-dimensional analysis of heat transfer in a micro-heat sink with single phase flow, Int. J. Heat Mass Transfer 47 (19–20) (2004) 4215–4231.

[16] M.D. Mikhailov, R.M. Cotta, S. Kakac, Steady state and periodic heat transfer in micro conduits, in: S. Kakac, L. Vasiliev, Y. Bayazitoglu, Y. Yener (Eds.), Microscale Heat Transfer—Fundamentals and Applications in Biological Systems and MEMS, Kluwer Academic Publisher, The Netherlands, 2005.

[17] C.P. Tso, S.P. Mahulikar, The role of the Brinkman number in analyzing flow transitions in microchannels, Int. J. Heat Mass Transfer 42 (10) (1998) 1813–1833.

[18] O. Aydin, M. Avci, Analysis of laminar heat transfer in micro-Poiseuille flow, Int. J. Thermal Sci. 46 (2007) 30–37.

[19] S. Kakac, Y. Yener, Convective Heat Transfer, second ed., CRC Press, Boca Raton, FL, 1995.

[20] S.V. Patankar, Numerical Heat Transfer and Fluid Flow, McGraw-Hill, New York, 1980.

[21] S.C. Shapra, R.P. Canale, Numerical Methods for Engineers, third ed., McGraw-Hill, New York, 1998.